OXYGEN ISOTOPIC COMPOSITION OF A COMETARY ENSTATITE RIBBON: EVIDENCE FOR CONDENSATION FROM ^{16}O–POOR GAS IN THE OUTER SOLAR SYSTEM R. C. Ogliore[1], J. B. Lewis[1], K. L. Utt[1], K. Nagashima[2], A. N. Krot[2], D. J. Joswiak[3], D. E. Brownlee[3]. [1]Department of Physics, Washington University in St. Louis, St. Louis, MO 63130, USA, [2]Hawai'i Institute of Geophysics and Planetology, University of Hawai'i at Mānoa, Honolulu, HI 96822, USA, [3]Department of Astronomy, University of Washington, Seattle, WA 98195, USA.

Introduction: Crystals with filamentary structure were predicted to condense directly from gas in the solar nebula and become incorporated into comets [1]. Whiskers, ribbons, and platelets of almost pure enstatite ($MgSiO_3$) were identified in chondritic-porous interplanetary dust particles (CP-IDPs) [2], and an enstatite whisker was identified in the Stardust samples from comet Wild 2 [3]. Whiskers and ribbons consist of only clinoenstatite elongated along the crystallographic [100] axis, and stacking defects are evidence of their vapor-phase growth [2] (Fig. 1). Filamentary enstatite appears to be relatively common in cometary material (CP-IDPs) (Fig. 1) but rare in relatively pristine asteroidal material (reported only in TEM studies of Paris (CM2) [4] and Bishunpur (LL3) [5]), implying these objects could be more abundant in the comet-forming region in the outer solar nebula and may have formed there. Therefore, filamentary enstatite in cometary IDPs could be a direct and pristine sample of outer nebula gas at the time of comet formation.

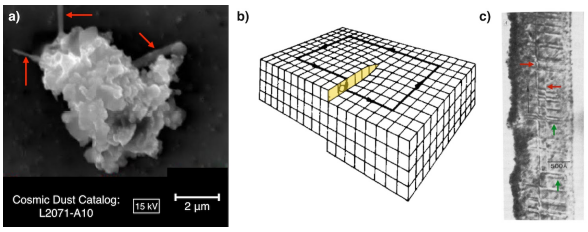

Figure 1: a) SE image of an IDP from NASA's Cosmic Dust Catalog with three probable enstatite whiskers. b) Schematic of crystal structure showing a screw dislocation. c) Bright-field TEM image of entstatite whisker showing screw dislocations (red arrows) and stacking faults (green arrows). Modified from [2].

Fine-grained, spinel-rich CAIs in primitive meteorites are known to be direct gas-to-solid condensates based on their Group II REE patterns [6], and thus record the O composition of inner nebula gas. Fine-grained CAIs that escaped subsequent alteration and O isotope exchange are ^{16}O-rich (though rare exceptions exist [7]), only slightly heavier than the O composition of the Sun (Δ^{17}O=-28.4 ± 1.8‰ [8]). Filamentary enstatite condensing from a gas of ∼solar composition in the outer nebula would also be ^{16}O-rich. In contrast, filamentary enstatite condensing in the outer nebula from a gas created by the vaporization of ^{16}O-poor dust [9] or a mixture of ^{16}O-rich dust and ^{16}O-poor water [10] would be ^{16}O-poor. Either process requires a heat source to vaporize dust in the outer nebula, such as within giant planet embryos [11]. Chondrule fragments [12] and CAIs [13] found in comet Wild 2 are thought to be transported from the inner nebula [14], or they may have formed in energetic processes in the outer nebula [15]. Analyses of a comet-specific phase will help determine if high-temperature processing occurred in the comet-forming region.

Methods: We identified an 800×200 nm ribbon in the giant cluster IDP U2-20GCA (Fig. 2). The ribbon was measured by SEM-EDS to be consistent with Fe-poor enstatite (Mg/Si ≈ 1, Fe/(Mg+Fe) < 0.05).

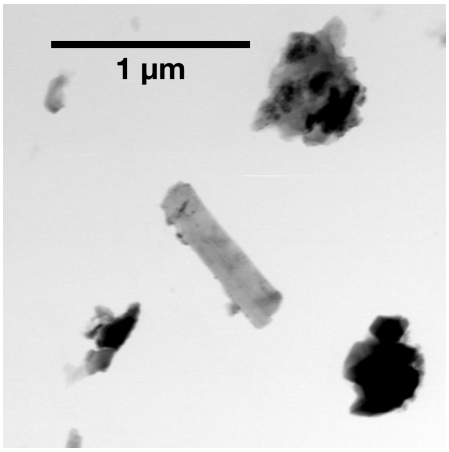

Figure 2: Bright-field TEM image of enstatite ribbon.

We transfered the enstatite ribbon from the TEM grid to a sputter-cleaned Au ion-probe mount using a computer-controlled Omniprobe needle in an FEI Quanta 3D FIB. We also transferred crushed grains of San Carlos olivine, an oxygen isotope standard, to within 10 μm of the enstatite ribbon so that both the standard and unknown could be measured simultaneously in one raster ion image (Fig. 3).

We acquired 10×10 μm, 256×256 pixel scanning ion images using the Cameca ims 1280 ion microprobe at the University of Hawai'i. We used a <3 pA Cs^+ primary beam focused to ∼250 nm. An electron flood gun was used for charge compensation. We simultaneously collected $^{16}O^-$, $^{17}O^-$, and $^{18}O^-$ on separate electron multipliers. Mass-resolving power for $^{17}O^-$ was ∼5500 to minimize contribution from $^{16}OH^-$. We also measured the $^{16}OH^-$ signal with electrostatic deflection

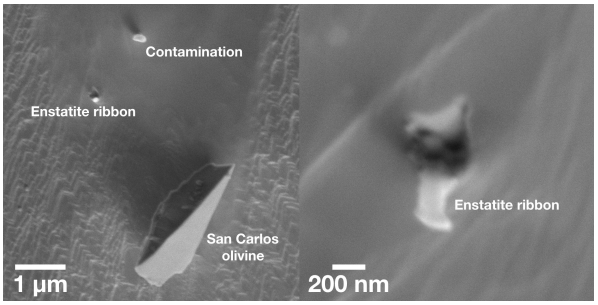

Figure 3: Enstatite ribbon mounted for O isotope analyses. The ribbon stuck to the Au mount nearly perpendicular to its surface.

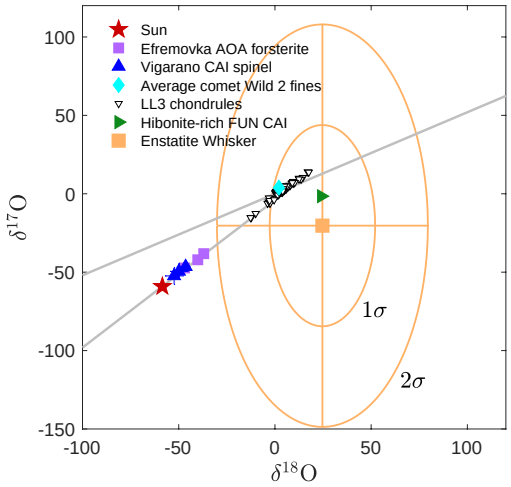

Figure 4: O composition of enstatite ribbon (orange) compared to the Sun [8], Efremovka AOA [16], Vigarano CAI [16], comet Wild 2 fines [17], LL3 chondrules [18], and a hibonite-rich FUN CAI [19].

(DSP2-x) to quantify any contribution of this interference to $^{17}O^-$. We collected 2000 frames (21 hours) then decreased the raster size to 2×2 μm for 200 frames (2.7 hr), then increased the raster back to 10×10 μm for another 200 frames. After these measurements, the enstatite ribbon was completely sputtered away. The total useful yield of O from the enstatite was $\sim$0.5%.

Data Analysis: We aligned the stack of 2400 isotope images for drift during the measurement, removed spurious cycles, then defined regions-of-interests around the enstatite whisker and San Carlos olivine. We corrected counts for deadtime and used San Carlos olivine to constrain the yields on the electron multipliers (EMs) used to measure $^{17}O^-$ and $^{18}O^-$. We did not see any change in the efficiency in any of the EMs over the course of the measurement because the count rates were relatively low ($<10^5$ cps). We removed the first 150 cycles as adsorbed water (background O) on the Au mount was removed. We calculated uncertainties by a bootstrap Monte Carlo method: we randomly resampled pixels in the enstatite ribbon region-of-interest 10^4 times and calculated the standard deviation of these trials. Monte Carlo uncertainties were $\sim$25% larger than statistical uncertainties. We assumed that the instrumental mass fractionation effects due to the height difference between the unknown and standard are small compared to measurement uncertainties.

Results: We measured the O isotopic composition of the enstatite ribbon to be: δ^{18}O=24.6$\pm$55.0, δ^{17}O=$-$20.5$\pm$129.0 (2σ). The enstatite ribbon is consistent with ^{16}O-poor compositions seen in chondrules but is not consistent, at the 2σ level, with the ^{16}O-rich compositions seen in unaltered gas-to-solid condensates found in the inner Solar System (Fig. 4).

Conclusions: Our measurements show that a cometary enstatite ribbon condensed from a ^{16}O-poor gas. The composition of this gas differs from the solar composition and was likely created by vaporization of primordial solids. Since filamentary enstatite is preferentially found in cometary material, it is most likely that this ribbon formed by high-temperature processing in the outer nebula, rather than being transported from the inner nebula. Abundance estimates and detailed TEM analyses of any filamentary enstatite found in meteorites combined with additional O isotope analyses will constrain the types of processing that occurred in the inner and outer solar nebula.

References: [1] B. Donn and G. W. Sears. *Science* 140.3572 (1963), 1208–1211. [2] J. P. Bradley, D. E. Brownlee, and D. R. Veblen. *Nature* 301 (1983), 473–477. [3] J. Stodolna et al. *Earth Planet. Sc. Lett.* 388 (2014), 367–373. [4] H Leroux et al. *Geochim. Cosmochim. Ac.* 170 (2015), 247–265. [5] H Leroux. *LPSC*. Vol. 43. 2012, p. 1761. [6] A. M. Davis and L. Grossman. *Geochim. Cosmochim. Ac.* 43.10 (1979), 1611–1632. [7] A. N. Krot et al. *Geochim. Cosmochim. Ac.* 201 (2017), 155–184. [8] K. D. McKeegan et al. *Science* 332.6037 (2011), 1528–1532. [9] A. N. Krot et al. *Astrophys. J.* 713.2 (2010), 1159. [10] C. M. O. Alexander et al. *Meteorit. Planet. Sci.* 52 (2017), 1797–1821. [11] S. Nayakshin, S.-H. Cha, and J. C. Bridges. *Mon. Not. R. Astron. Soc. Let.* 416.1 (2011), L50–L54. [12] R. C. Ogliore et al. *Astrophys. J. Lett.* 745.2 (2012), L19. [13] D. J. Joswiak et al. *Meteorit. Planet. Sci.* (2017). [14] F. J. Ciesla. *Science* 318.5850 (2007), 613–615. [15] J. C. Bridges et al. *Earth Planet. Sc. Lett.* 341 (2012), 186–194. [16] A. N. Krot et al. *Science* 295.5557 (2002), 1051–1054. [17] R. C. Ogliore et al. *Geochim. Cosmochim. Ac.* 166 (2015), 74–91. [18] N. T. Kita et al. *Geochim. Cosmochim. Ac.* 74.22 (2010), 6610–6635. [19] L Kööp et al. *LPSC*. Vol. 46. 2015, p. 2750.